



# Bone microstructure supports a Mesozoic origin for a semiaquatic burrowing lifestyle in monotremes (Mammalia)

Suzanne J. Hand<sup>a,1</sup> , Laura A. B. Wilson<sup>a,b,c,1</sup> , Camilo López-Aguirre<sup>d,e,f</sup> , Alexandra Houssaye<sup>g</sup> , Michael Archer<sup>a</sup> , Joseph J. Bevitt<sup>h</sup> , Alistair R. Evans<sup>i</sup> , Amalia Y. Halim<sup>k</sup>, Tzong Hung<sup>l</sup>, Thomas H. Rich<sup>j</sup> , Patricia Vickers-Rich<sup>m</sup> , and Robin M. D. Beck<sup>n</sup>

Affiliations are included on p. 10.

Edited by Zhe-Xi Luo, The University of Chicago, Chicago, IL; received July 8, 2024; accepted March 22, 2025 by Editorial Board Member David Jablonski

The platypus and four echidna species are the only living egg-laying mammals and the sole extant representatives of Order Monotremata. The platypus and echidnas are very disparate both morphologically and ecologically: The platypus is a specialized semiaquatic burrowing form that forages for freshwater invertebrates, whereas echidnas are fully terrestrial and adapted for feeding on social insects and earthworms. It has been proposed that echidnas evolved from a semiaquatic, platypus-like ancestor, but fossil evidence for such a profound evolutionary transformation has been lacking, and this hypothesis remains controversial. Here, we present original data about the Early Cretaceous (108 to 103 Ma) Australian mammal *Kryoryctes cadburyi*, currently only known from a single humerus, that provides key information relating to this question. Phylogenetic analysis of a 536-character morphological matrix of mammaliaforms places *Kryoryctes* as a stem-monotreme. Three-dimensional whole bone comparisons show that the overall shape of the humerus is more similar to that of echidnas than the platypus, but analysis of microstructure reveals specializations found in semiaquatic mammals, including a particularly thick cortex and a highly reduced medullary cavity, present in the platypus but absent in echidnas. The evidence suggests *Kryoryctes* was a semiaquatic burrower, indicating that monotremes first evolved an amphibious lifestyle in the Mesozoic, and providing support for the hypothesis that this is ancestral for living monotremes as a whole. The lineage leading to the modern platypus appears to have been characterized by extremely long term (>100 My) niche conservatism, with echidnas representing a much later reversion to a fully terrestrial lifestyle.

bone microstructure | Mesozoic | monotreme | semiaquatic burrowing | Gondwana

The platypus (*Ornithorhynchus anatinus*, family Ornithorhynchidae) of eastern Australia and the four species of echidna (*Tachyglossus aculeatus* and three species of *Zaglossus*, family Tachyglossidae) of Australia and New Guinea are the only living representatives of the mammalian order Monotremata (1, 2). Monotremes have played a central role in our understanding about mammalian evolution because of their position as the extant sister-taxon of placentals and marsupials (which collectively comprise the remaining ~6,000 living mammal species) and their retention of several plesiomorphic traits, of which the most striking is oviparity (egg-laying). However, much remains unknown or controversial about the evolutionary history of monotremes, in large part because of their very incomplete fossil record and because none of the living species retains functional teeth, making it difficult to compare them to fossil mammals, most of which are only known from dental remains (3).

The platypus and echidnas differ strikingly from each other, both morphologically and ecologically. The platypus is a semiaquatic form with specializations including dense, waterproof fur, extensively webbed feet, a large, beaver-like tail, and a broad, soft, electroreceptive bill that is used to forage for freshwater invertebrates (4). By contrast, echidnas are fully terrestrial (although they are capable of swimming), lack waterproof fur and webbed feet, and have a very short tail (5). Echidnas are covered in spines dorsally and laterally, and have a narrow, elongate, toothless snout terminating in a tiny terminal mouth; a long, extensible tongue is used to collect social insects in the case of the short-beaked echidna, *T. aculeatus* (5), or earthworms in the case of the long-beaked echidnas, species of *Zaglossus* (6).

Despite these striking differences, several studies have proposed that echidnas evolved from a semiaquatic, platypus-like ancestor (7–13). Indirect support for this hypothesis comes from a variety of sources. Several molecular clock studies suggest that the platypus and echidna lineages probably diverged from each other during the Cenozoic (12, 14–18), as do recent morphological tip-dating analyses (19–21). Two fossil monotremes from the Cretaceous of Australia, *Steropodon galmani* (from the ~100 Ma Griman Creek Formation

## Significance

The egg-laying monotremes have played a central role in our understanding of mammalian evolution, but their fossil record is poor and their evolutionary history is controversial. Living monotremes are ecologically very distinct from each other: The platypus is well adapted for a semiaquatic lifestyle, whereas echidnas are fully terrestrial. Here, we show that an isolated mammal humerus from the Early Cretaceous of Australia, from a species called *Kryoryctes cadburyi*, belongs to a monotreme, and that microscopic features of this bone indicate that this monotreme was a semiaquatic burrower. This suggests that the amphibious lifestyle of the modern platypus had its origins at least 100 Mya, during the Age of Dinosaurs, and that echidnas evolved from semiaquatic ancestors.

Author contributions: S.J.H., L.A.B.W., C.L.-A., M.A., and R.M.D.B. designed research; L.A.B.W., C.L.-A., A.H., M.A., J.J.B., A.R.E., A.Y.H., T.H., and R.M.D.B. performed research; A.H., J.J.B., A.R.E., A.Y.H., and T.H. contributed new reagents/analytic tools; L.A.B.W., C.L.-A., A.H., J.J.B., A.R.E., A.Y.H., T.H., T.H.R., P.V.-R., and R.M.D.B. analyzed data; and L.A.B.W., C.L.-A., A.H., M.A., J.J.B., A.R.E., T.H.R., P.V.-R., and R.M.D.B. wrote the paper.

The authors declare no competing interest.

This article is a PNAS Direct Submission. Z.-X.L. is a guest editor invited by the Editorial Board.

Copyright © 2025 the Author(s). Published by PNAS. This open access article is distributed under Creative Commons Attribution-NonCommercial-NoDerivatives License 4.0 (CC BY-NC-ND).

Although PNAS asks authors to adhere to United Nations naming conventions for maps (<https://www.un.org/geospatial/mapsgeo>), our policy is to publish maps as provided by the authors.

<sup>1</sup>To whom correspondence may be addressed. Email: s.hand@unsw.edu.au or laura.wilson@anu.edu.au.

This article contains supporting information online at <https://www.pnas.org/lookup/suppl/doi:10.1073/pnas.2413569122/-/DCSupplemental>.

Published April 28, 2025.

at Lightning Ridge, New South Wales) (2, 22) and *Teinolophos trusleri* (from the ~126 Ma Wonthaggi Formation at Flat Rocks, Victoria) (23), considerably predate these clock estimates, and yet both have enlarged canals in their lower jaws for the mandibular nerve (2, 22–24). This derived feature is likely indicative of electroreception (2, 24, 25) and may be an indication that *Steropodon* and *Teinolophos* fed in a similar manner to the living platypus, by semiaquatic foraging. Most phylogenetic analyses place *Steropodon* and *Teinolophos* outside the monotreme crown-clade (12, 19–21, 26–28), suggesting that electroreceptive capability (and hence possibly a semiaquatic lifestyle) may be plesiomorphic features retained by crown-monotremes. However, *Teinolophos* retains incisors and a canine, and appears to lack a true platypus-like bill (2, 23–25), and echidnas also have some electroreceptive capability that may be used in foraging (5, 11), showing that electroreception is not necessarily indicative of semiaquatic habits. Marginal cartilages present in embryos of the short-beaked echidna have been argued to represent vestiges of a platypus-like bill that has been lost secondarily (29, 30). Last, a comparative study of myoglobin surface charge in aquatic, semiaquatic, and terrestrial mammals found evidence that echidnas may have had a semiaquatic, diving ancestry (13). However, the hypothesis that echidnas evolved from semiaquatic, platypus-like ancestors has been challenged by some authors (24, 31, 32), and direct fossil evidence for this proposed evolutionary transformation has so far been lacking.

*Kryoryctes cadburyi* is a mammaliaform from the Early Cretaceous Slippery Rocks locality at Dinosaur Cove in southern Victoria (33, 34), currently known from a single humerus (35), with a single

partial premolar possibly also referable to the taxon (2, 33). It is the only Australian Mesozoic mammaliaform species represented by postcranial material, with morphological similarities to monotremes (particularly echidnas) noted in the original description (2, 35). Here, we present original data about the humerus of *Kryoryctes* (Figs. 1–4) that provide direct insight into the timing of the evolution of semiaquatic behavior in monotremes: specifically, phylogenetic analyses which indicate that *Kryoryctes* is a stem-monotreme, and qualitative and quantitative analyses of bone microstructure that provide evidence it was a semiaquatic burrower. We conclude that monotremes had evolved an amphibious lifestyle more than 100 Mya.

## Results

**Phylogenetic Relationships of *Kryoryctes*.** Maximum parsimony analysis of a 536 morphological character matrix of 71 mammal and mammaliaform taxa and six cynodont outgroup taxa (modified from Huttenlocker et al. (38); see *Materials and Methods*, *SI Appendix*, and *Dataset S1*) recovers two most parsimonious trees (length = 2,398 steps), both of which place *Kryoryctes* sister to Monotremata; the strict consensus of these is shown in Fig. 1. The *Kryoryctes*+Monotremata clade is not strongly supported (bootstrap < 50%; see *SI Appendix*, Fig. S1), probably because of the very few characters that could be scored for *Kryoryctes* in this matrix (17 of 536 characters, rendering it only 3.2% complete). However, maximum parsimony optimization of the morphological character matrix on the strict consensus indicates that the clade

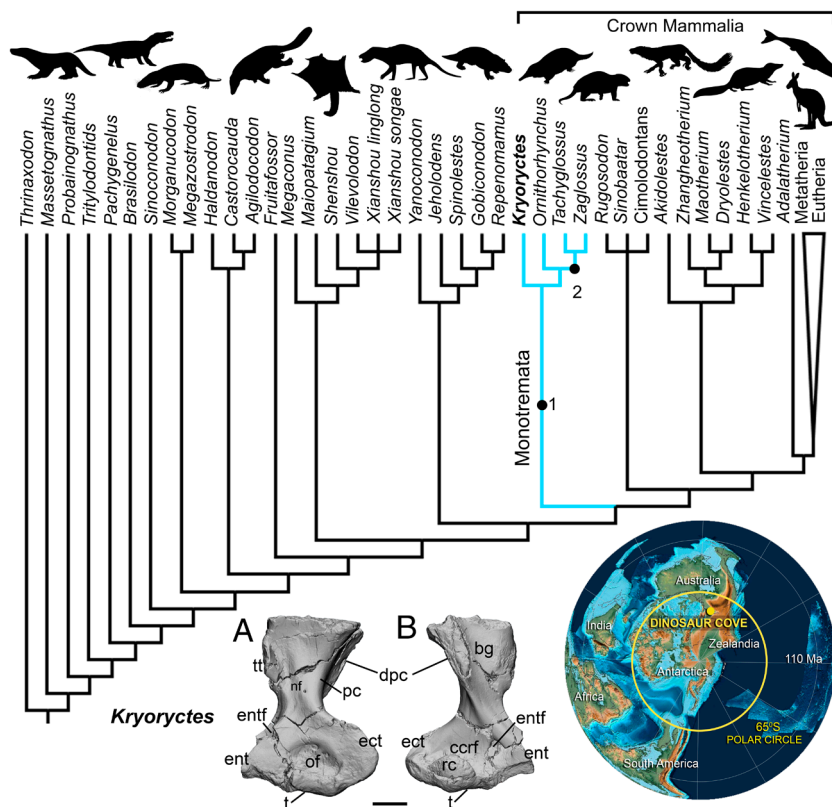


**Fig. 1.** Phylogenetic relationships of *K. cadburyi* among mammaliaforms. Strict consensus of two most parsimonious trees (length = 2,398 steps) that result from maximum parsimony analysis of a 71 taxon, 536 character (512 parsimony-informative, 105 ordered) morphological matrix (see also *SI Appendix*, Fig. S1); branch lengths are arbitrary. 1) inferred origin of semiaquatic lifestyle; 2) secondary loss of semiaquatic lifestyle. Other images: model of the type of *K. cadburyi* (NMV P208094 right humerus) in A, dorsal and B, ventral views; austral projection of the world 110 Ma, generated using GPlates (36) and showing fossil locality Dinosaur Cove, Victoria within the southern polar circle. Mammaliaform silhouettes from PhyloPic. Abbreviations: bg, bicipital groove; ccrf, combined coronoid and radial fossa; dpc, deltopectoral crest; ect, ectepicondyle; ent, entepicondyle; entf, entepicondyle fossa; nf, nutrient foramen; of, olecranon fossa; pc, posterior crest; rc, radial condyle; t, trochlear form articulation for ulna; tt, teres tubercle. (Scale bar represents 10 mm.)

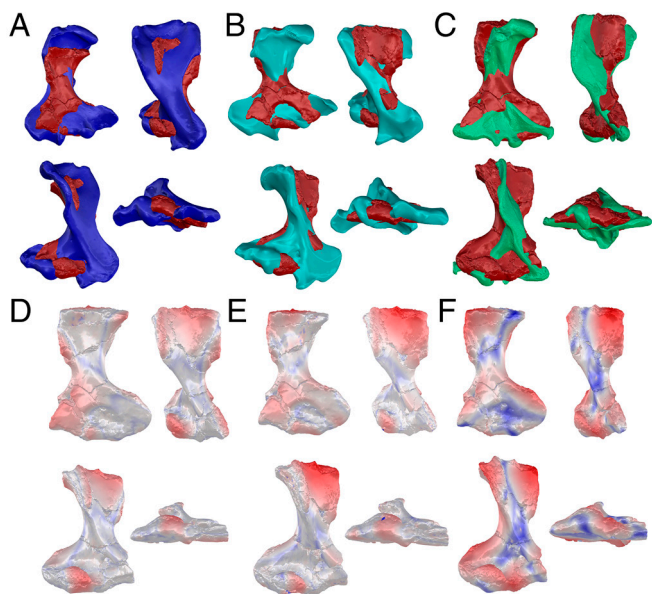


**Fig. 2.** *Kryoryctes* humeral shape compared with extant monotremes. (A–C) Mesh–mesh comparison of 3D digital models of *K. cadburyi* NMV P208094 (russet) with (A) *Zaglossus bruijnii* NMV C11586 (violet), (B) *T. aculeatus* NMV C2562 (teal) and (C) *O. anatinus* NMV C11285 (green); right humerus shown in dorsomedial, ventral, ventrolateral, and distal views. (D and E) Mesh–mesh deviation of 3D digital models of *Kryoryctes* with respect to extant monotreme humeri with areas of greatest deviation from *Kryoryctes* shown in red to blue ( $-7.177 \gg 2.183$ ); right humerus shown in dorsomedial, ventral, ventrolateral, and distal views. (D) *Z. bruijnii*; (E) *T. aculeatus*; (F) *O. anatinus*. See also *SI Appendix*, Figs. S3 and S4, and <https://figshare.com/s/c6e0a6909a2462d4db11> (37).

is characterized by two synapomorphies, namely: teres tuberosity on medial side of humerus hypertrophied (character 267, state 2; consistency index [ci] = 0.222); and width of distal humerus >50% total humeral length (character 544, state 1; ci = 0.333).

Monophyly of crown Monotremata (i.e., *Ornithorhynchus*+*Tachyglossus*+*Zaglossus*), to the exclusion of *Kryoryctes*, receives strong support (bootstrap = 84%) and is characterized by three unambiguous synapomorphies: olecranon fossa on dorsal face of humerus absent (character 539, state 1; ci = 0.2); orientation of the interepicondylar axis with respect to long axis of humerus oblique rather than perpendicular (character 542, state 1; ci = 0.333); and humeral contribution to elbow joint laterally positioned (character 543, state 1; ci = 0.2). *Kryoryctes* lacks all three of these apomorphies, and in this respect its humerus is less specialized than in extant monotremes and more closely resembles that of other mammaliaforms, including morganucodontans, docodontans, multituberculates, and therians (3, 39). Phylogenetically, the short, broad humerus of *Kryoryctes* and extant monotremes appears to be apomorphic for the clade. Generally, mammaliaforms have a more gracile humerus than monotremes (*SI Appendix*, Fig. S2; see also ref. 40), with exceptions in independent lineages of species interpreted to be burrowers and/or swimmers (e.g., the Mesozoic nonmammalian mammaliaforms *Fruitafossor* and *Haldanodon*, and the extant talpid mole *Talpa*; *SI Appendix*, Fig. S2). A short, robust humerus also occurs in some nonmammaliaform cynodonts (e.g., *Thrinaxodon*; *SI Appendix*, Fig. S2) and more distantly related synapsids (e.g., *Ophiacodon*, *Dimetrodon*, *Lystrosaurus*) (41), but these lack several derived features that place *Kryoryctes* with monotremes, within Mammaliaformes (*SI Appendix*, Table S1).

**Shape Comparisons of the *Kryoryctes* Humerus with Other Monotremes.** The holotype of *K. cadburyi*, a right humerus (NMV P208094) with broadly expanded proximal and distal extremities, a “waisted” or dumbbell-like appearance, and marked

torsion (>40% degree offset between orientation of the dorsal face of the proximal vs. distal end of the humerus) between the extremities, has been described in detail by Pridmore et al. (35) (see also *SI Appendix*). It is approximately 46 mm long, but is damaged, with the proximal portion (including the humeral head) missing (Fig. 1 and *SI Appendix*, Fig. S3); when fully intact, it is estimated to have been ~51 mm long (35). This is almost identical to adult maximum humeral length in *T. aculeatus* (mean = 49.7 mm, SD = 4.91, N=26), markedly larger than in *O. anatinus* (mean = 29.8 mm, SD = 3.6, N = 13), and smaller than in *Z. bruijnii* (mean = 72.6 mm, SD = 1.5, N = 2) and *Z. bartoni* (65.3 mm based on a single individual) (*SI Appendix*, Table S2). Based on this, and the overall close resemblance in humeral shape between NMV P208094 and living monotremes, we conclude that the body mass of *Kryoryctes cadburyi* was probably similar to that of *T. aculeatus*, approximately 2.5 to 5 kg (42).

Virtual comparison of 3D digital models of the microCT-scanned humerus of *Kryoryctes* with those of extant monotremes (*Materials and Methods* and *SI Appendix*, Fig. S4, 3D models <https://figshare.com/s/c6e0a6909a2462d4db11>) (37) indicates a closer alignment of mesh shape between *Kryoryctes* and echidnas (Fig. 2 A and B) than with the platypus (Fig. 2C). Based on comparison of mesh–mesh deviation results, this shape comparison also indicates that NMV P208094 shows the greatest resemblance to *Zaglossus* (Fig. 2D), rather than to *Tachyglossus* (Fig. 2E). Intermodel distances between *Kryoryctes* and *Zaglossus* were  $-4.43$  (maximum negative excursion) to  $0.97$  (maximum positive excursion), compared to those between *Kryoryctes* and *Tachyglossus* ( $-7.18$  to  $2.18$ ) and *Ornithorhynchus* ( $-7.80$  to  $2.21$ ). The areas of greatest deviation between meshes of *Kryoryctes* and extant monotremes correspond to the greater degree of proximal flexion of the humerus in the echidnas (Fig. 2 D and E); the greater humeral torsion in the platypus (Fig. 2F); and the bulbous, combined condyle for the radius and ulna in the platypus and echidnas (Fig. 2 D–F).

**Humeral Microstructure of *Kryoryctes* and Living Monotremes Compared to Other Mammals.** MicroCT scan data of NMV P208094 (*Materials and Methods*) reveals that the cortex (bone wall) of the humerus of *Kryoryctes* is relatively thick throughout the length of the shaft (Fig. 3 A and E). It is thickest at the mid-diaphysis, around the growth center (Fig. 4A), but cortical thickening also occurs in the proximity of muscle attachment sites (deltopectoral crest, teres tubercle on greater tubercular ridge, posterior crest, and lateral epicondylar crest; Figs. 3 A and E and 4A). The *Kryoryctes* humerus lacks a true open medullary cavity: The medullary area is filled by osseous trabeculae whose compactness strongly diminishes toward the ossification center, where the originally periosteal region has a few thick trabecular struts and large intertrabecular spaces. The trabecular bone of endochondral origin exhibits thinner trabeculae and smaller intertrabecular spaces, forming a more homogeneous spongiosa (Figs. 3 A and E and 4A). In the distal epiphysis (the proximal epiphysis of the specimen is missing), trabeculae are more numerous and thinner (Fig. 3E). A large nutrient canal that can be traced across the cortex into the central trabecular network confirms the position of the bone growth center, used for analysis in Bone Profiler (43).

Compared to *Kryoryctes*, the humerus of *Ornithorhynchus* has a much thicker cortex (Fig. 3 B and F), although there appears to be variation in cortical thickness among platypus individuals (compare Fig. 4 B and C). In three of the four *Ornithorhynchus* specimens that we examined, there is an open medullary cavity but the rest of the bone essentially consists of compact bone (see also ref. 44, figure 12A), except for a few cavities crossed by

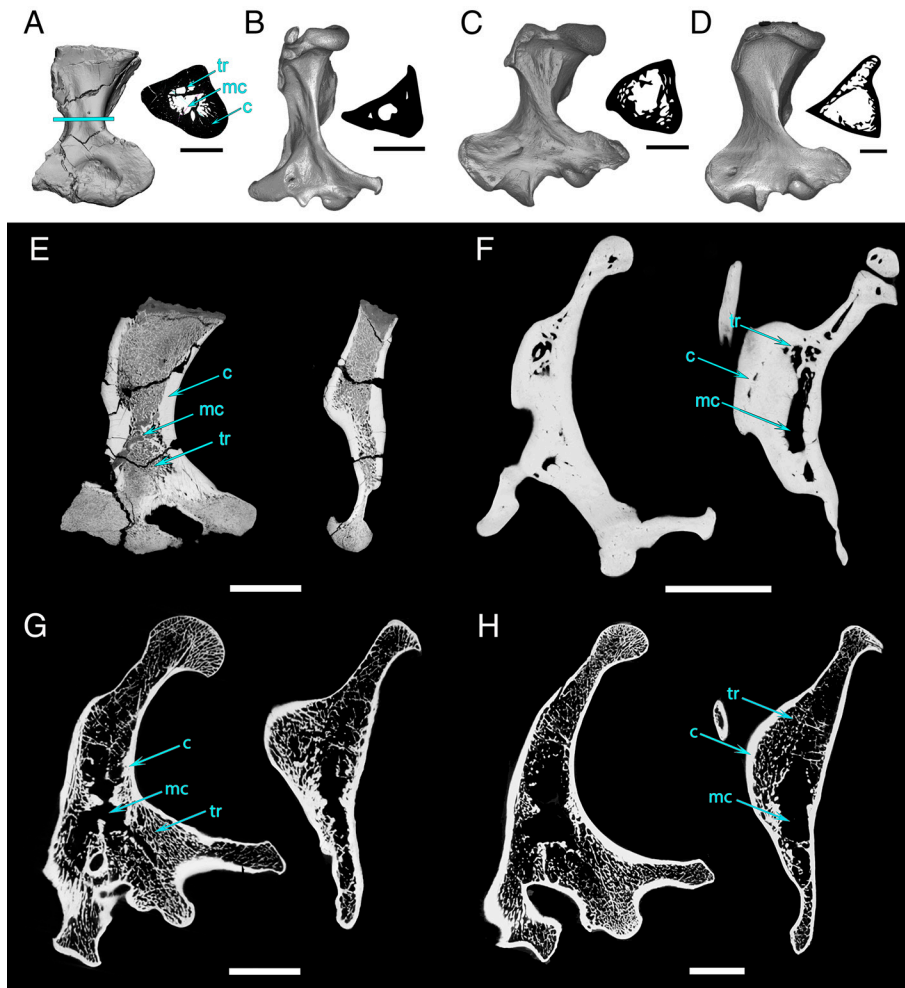


**Fig. 3.** *Kryoryctes* humeral bone microstructure compared with extant monotremes. (A–D) Right humeri 3D models in dorsomedial view and binary images of virtual cross-sections at the mid-diaphysis of the humerus of (A) *K. cadburyi* NMV P208094 and extant monotremes, (B) *O. anatinus* NMV C11285, (C) *T. aculeatus* NMV C2562 and (D) *Z. bruijini* NMV C11586. Scale bars for cross-sections represent 5 mm. Solid line (aqua) indicates location of cross-sections. See also *SI Appendix, Fig. S2*. (E–H) Humerus 3D virtual longitudinal coronal (Left) and sagittal (Right) sections of (E) *K. cadburyi* NMV P208094; (F) *O. anatinus* NMV C11285; (G) *T. aculeatus* NMV C2562; and (H) *Z. bruijini* NMV C11586. See also *SI Appendix, Fig. S10*. Scale bars for longitudinal sections represent 10 mm. Abbreviations: c, cortex; mc, medullary cavity; tr, trabecula.

relatively thick struts toward the epiphyses; even the epiphyses are strongly compact, with no true trabecular bone in the entire bone (Fig. 3F). In the fourth specimen (UNSW AR22921; Fig. 4C), the medullary area at mid-diaphysis is much larger (Fig. 4C and see also ref. 45, figure 2K). Differences in femoral histology, including the size of the medullary cavity, between platypus individuals examined in other studies (46, 47) have also been noted (46). Microanatomical variation may be considerable in the long bones of the modern platypus, but whether this diversity might relate to age, sex, reproductive status, egg laying, seasonality, or captive versus wild-caught individuals is currently unknown.

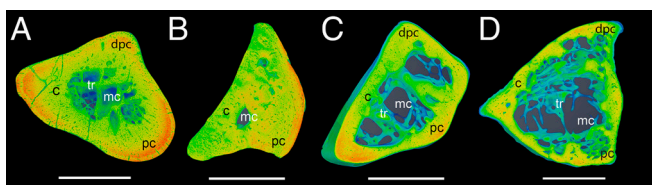


**Fig. 4.** 3D virtual cross-sections of monotreme humeri at mid-diaphysis. (A) *K. cadburyi* NMV P208094; (B) *O. anatinus* UNSW AR22920; (C) *O. anatinus* UNSW AR22921; (D) *T. aculeatus* UNSW AR22922. Relative density scale: red (highest density) to violet (lowest). Scale bars represent 5 mm. Section blocks 700  $\mu\text{m}$ , except B which is 500  $\mu\text{m}$ . Abbreviations: c, cortex; dpc, deltopectoral crest; mc, medullary cavity; pc, posterior crest; tr, trabecula.

By contrast, the humeri of the tachyglossids *T. aculeatus* and *Z. bruijini* have a much wider medullary area and thinner cortex, this thickness being relatively homogeneous along the entire bone, especially in *Zaglossus* (Fig. 3 G and H). Trabecular bone extends beyond the metaphyses into the diaphysis, but it is relatively loose with fine trabeculae, and the core of the bone is occupied by an open medullary cavity. The medullary cavity is relatively void of bone in *Zaglossus* (Fig. 3 D and H), whereas some remains of cortical bone extend in the diaphysis near the growth center in *Tachyglossus*, resulting in the relative thickening of the cortex in this area (Fig. 3 C and G). Although humeral cortical thickness varies conspicuously among platypus individuals (e.g., Fig. 4 B and C and *SI Appendix, Fig. S5*), it is still much greater than that in tachyglossids (e.g., Fig. 4D and *SI Appendix, Fig. S5*), and the few, thick trabeculae crossing the medulla and large intratrabecular spaces found in some platypuses, and in *Kryoryctes*, also contrasts sharply with the vacant medulla in echidnas.

**Quantitative Analysis of Humeral Microstructure and Ecology.** Bone microstructure at the mid-diaphysis was analyzed for the humeri of *Kryoryctes*, *Ornithorhynchus*, *Tachyglossus*, and *Zaglossus* using the software Bone Profiler (43) (*Materials and Methods, Fig. 5*, and *SI Appendix, Fig. S5*) for the parameters C (the area of compact bone), P (a measure proportional to the

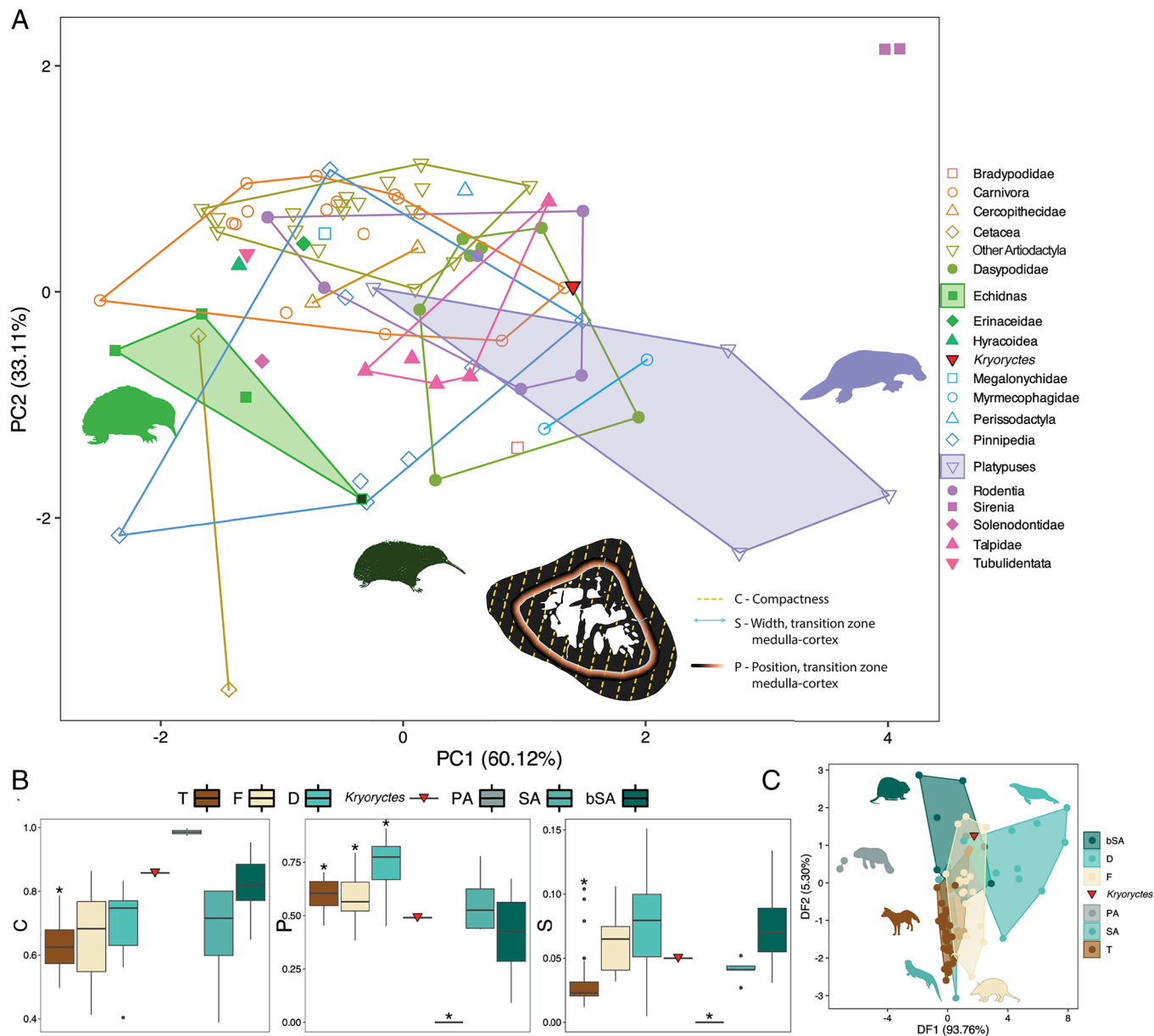


**Fig. 5.** Bone microstructure attributes of *Kryoryctes* compared with extant mammals. (A) Results of PCA showing variance along PC1 and PC2 for all mammal taxa examined (data and abbreviations in *SI Appendix, Table S4*) and convex hulls for taxon groups, except Sirenia (see top right), indicated in legend. (Inset) cross-section of *K. cadburyi* humerus NMV P208094 with a visual overview of the parameters, C, P, and S, measured in this study, using Bone Profiler program (43). C, bone compactness, is calculated by dividing the total area of the section comprising bone tissue (black area with yellow dashes) by the total area of the cross-section. S, is proportional to the relative width of the transition zone between the medulla and cortex (blue arrows show the width of the transition zone), and P generally represents the position of the transition zone between the medullary and cortical regions (gradient colored line, for illustration of approximate location). P, S, and C are parameters of a model with the distribution of mineralized tissue as a function of the distance from the center of the bone. See ref. 52 for further details. (B) Boxplots for parameters C, P, and S for six habit categories (legend), where T, terrestrial; F, fossorial; D, essentially or exclusively aquatic deep divers; PA, exclusively aquatic poorly active swimmers; bSA, burrowing semiaquatic shallow swimmer or diver; SA, semiaquatic shallow swimmer or diver (see also *SI Appendix, Table S4*). The asterisk indicates significant difference in mean from bSA mean (Dunnett's pairwise comparisons; *SI Appendix, Table S5*). (C) Results of LDA showing variance along LD1 and LD2 for six habit categories (see also *SI Appendix, Tables S6 and S7*). Mammal silhouettes from PhyloPic.

size of medullary cavity), and S (the width of the transition zone between the cortical bone and the medullary cavity). The cross-sectional compactness of the humerus of *Kryoryctes* is  $C = 0.86$ . This value exceeds the threshold for osteosclerotic bone (0.82) as defined for mammalian ribs (48), and is in the range observed in the humeri of extant mammals that are amphibious [0.65 to 0.95 (49)], including the humeri of *O. anatinus* (*SI Appendix, Table S4*). Conversely, compactness is lower in the humeri of *Tachyglossus* (0.53 to 0.58), and especially, *Zaglossus* (0.41; *SI Appendix, Table S4*) which is particularly low compared to the mean value of 0.57 for humeri of terrestrial mammals (50, 51).

In monotremes, humeral cortical thickness does not appear to scale with size, robusticity, or torsion, unlike in (e.g.) nonmammalian cynodonts (53) (*SI Appendix, Fig. S7*). Among monotremes, *Ornithorhynchus* has the smallest humeral shaft diameter and thickest cortex, whereas *Zaglossus* species have the greatest humeral shaft diameter yet thinnest cortex (Figs. 4 and 5, and *SI Appendix, Fig. S5*). Although their humeri are similar in size, in *Tachyglossus* torsion is greater, but its cortex is thinner than in *Kryoryctes* (Figs. 4 and 5 and *SI Appendix, Fig. S5*).

We compared the bone microstructure parameters C, P, and S in *Kryoryctes* with 82 living mammals of known ecology. We used the habit categories of Hayashi et al. (49), i.e., terrestrial (T; e.g.,

**Table 1. Predicted lifestyle of *Kryoryctes* and the most recent common ancestor (MRCA) of crown Monotremata+*Kryoryctes* (CM+K) from linear discriminant analyses (LDA) using equal priors, in which humeral microstructure attributes (values of C, P, S) of *Kryoryctes* were compared with those of 82 living mammals of known ecology (bSA, D, F, PA, SA, T; after Hayashi et al. (50) and this paper)**

	bSA	D	F	PA	SA	T
Predicted lifestyle of <i>Kryoryctes</i> : bSA						
	0.567	0.016	0.328	4.66E-17	0.067	0.023
Predicted lifestyle of MRCA of crown Monotremata+ <i>Kryoryctes</i> : bSA						
CM+K_0.001 Ma	0.567	0.016	0.328	4.66E-17	0.067	0.023
CM+K_1 Ma	0.563	0.015	0.331	4.96E-17	0.068	0.023
CM+K_5 Ma	0.539	0.011	0.347	6.64E-17	0.076	0.027
CM+K_10 Ma	0.515	0.008	0.361	9.14E-17	0.085	0.031
CM+K_20 Ma	0.465	0.004	0.386	1.76E-16	0.104	0.040

Values are posterior probabilities (see also *SI Appendix, Table S8*). For the MRCA, posterior probabilities are for five simulations of different phylogenetic branch lengths leading to *Kryoryctes* (*Materials and Methods, Fig. 1, and SI Appendix, Fig. S9*).

*Felis*), fossorial (F; e.g., *Talpa*), essentially or exclusively aquatic deep divers (D; e.g., *Phoca*), and exclusively aquatic poorly active swimmers (PA; e.g., *Dugong*), but because the platypus swims and also burrows; we split their semiaquatic shallow swimmer or diver category into semiaquatic burrowers (bSA; species of *Ornithorhynchus*, *Myocastor*, *Ondatra*, *Amblonyx*, *Lutra*; *SI Appendix, Fig. S6*) and semiaquatic nonburrowers (SA; e.g., sea otter) (*Materials and Methods and SI Appendix, Table S4 and Fig. S6*).

The results of a PCA are given in Fig. 5A (and *SI Appendix, Fig. S8* with taxon labels). The first two axes of the PCA explain 93.23% of the total variance in the sample, with the first axis explaining 60.12%, and the second 33.11%. PC1 mostly expresses the distribution of the variance according to the parameters C and P. It is mostly positively correlated with C (loading 0.71) and negatively correlated with P (loading -0.69). PC2 largely represents variation in S (loading 0.98), and to a much lesser extent P (loading 0.18).

PC1 separates *Trichechus manatus* (manatee) and *Dugong dugon* (dugong), which are fully aquatic but poorly active swimmers (PA), from other taxa other than one platypus specimen (Fig. 5A and S5). This result reflects the strong osteosclerosis and absence of a true open medullary cavity in the humeri of these species (high values of C and low P values; *SI Appendix, Fig. S6E*). Three of the four specimens of the semiaquatic burrowing *O. anatinus* included in our study are also clearly distinguished from other taxa on this axis, one of them grouping with the sirenians (Fig. 5A). Along PC1, the opposite trend is seen in taxa with a spongy organization in their humerus, and thus relatively thin cortex; the more negative values in our analysis include the aquatic and deep diving *Mirounga leonina* (elephant seal; *SI Appendix, Fig. S6A*), and the semiaquatic nonburrowing *Ursus maritimus* (polar bear; *SI Appendix, Fig. S6O*), but also the terrestrial *Zaglossus bruijnii* (long-beaked echidna). Along PC2, sirenians are separated from all other taxa, and at the opposite (positive) end of the axis *Delphinus delphis* (common dolphin; *SI Appendix, Fig. S6B*) is distinct, largely on the basis of its wider medullary area and more gradual transition between the cortex and medulla.

*K. cadburyi* separates from *Ornithorhynchus*, *Tachyglossus*, and *Zaglossus*, but lies closer in morphospace to the platypus than to the echidnas. Among all our taxa, it lies closest to the sea otter *Enhydra lutris* (*SI Appendix, Figs. S6N and S8*).

Boxplots for parameters C, P, and S for the six habit categories (D, F, T, SA, bSA, PA) show that the compactness of the *Kryoryctes*

humerus is higher than in diving, semiaquatic nonburrowing, terrestrial, and most fossorial mammals, but lower than in sirenians (PA), and falls within the third quartile for semiaquatic burrowing mammals (Fig. 5B). Its P value (a measure proportional to the width of the medullary cavity) overlaps with most groups except sirenians, but is closest to the medians for semiaquatic and semiaquatic burrowing mammals. This is also the case for its S value (width of transition zone between cortex and medullary cavity).

Dunnnett's pairwise comparisons of the means of C, P, and S for the different ecologies showed statistically significant differences between semiaquatic mammals (burrowing and/or nonburrowing) and all other categories, and no significant difference between *Kryoryctes* and semiaquatic mammals (burrowing and/or nonburrowing) (*SI Appendix, Table S5*).

In our LDA using the lifestyle six-state coding of T, SA, bSA, PA, D, and F, *Kryoryctes* lies within the convex hulls of bSA, D, and F (Fig. 5C). This model correctly attributed the lifestyle of 69.5% of extant mammalian comparative species of known ecology (*SI Appendix, Tables S6 and S7*). The predicted habit for *Kryoryctes* was identified as semiaquatic burrowing (bSA) with a posterior probability of 56.7%, which is 1.7× higher than the probability that it had a strictly fossorial habit (32.81%; Table 1).

LDA including ancestral state reconstructions for variables C, P, and S predicted the most probable ancestral lifestyle for the MRCA of crown Monotremata without *Kryoryctes* in the tree to be fossorial (52% posterior probability), followed by semiaquatic and semiaquatic burrowing (each 19% posterior probability; *SI Appendix, Table S8*). With *Kryoryctes* added, the most probable ancestral lifestyle for crown Monotremata was still fossorial (47% to 50% posterior probability depending on branch length leading to *Kryoryctes*), but support for a semiaquatic lifestyle was almost identical (combined 43% to 47% posterior probability, with 28% to 34% for burrowing semiaquatic and 13% to 15% nonburrowing semiaquatic). There was also strong support for a semiaquatic ancestral lifestyle of the MRCA of Monotremata + *Kryoryctes* (47% to 57%, depending on the branch lengths leading to *Kryoryctes*), with fossorial less likely (33% to 39%; Table 1).

Overall, our quantitative results indicate that *Kryoryctes* had a semiaquatic, and specifically a semiaquatic burrowing lifestyle, rather than a fossorial, terrestrial, diving, or slow moving exclusively aquatic lifestyle, and that the most recent common ancestor of crown Monotremata+*Kryoryctes* was probably also a semiaquatic burrower.

**Phylogenetic Signal in Humeral Bone Microstructure.** Based on Upham et al.'s (16) node-dated molecular phylogeny of mammals (modified here by pruning species and adding the fossil *Kryoryctes*), and using Moran's I index of autocorrelation (*Materials and Methods*), we found significant phylogenetic signal in our compiled sample of 82 mammalian humeri for the bone microstructure parameters C, P, and S. Values for most indices (Cmean, I, K, K.star, Lambda) were statistically significant for all three variables (*SI Appendix, Table S9*). However, support was generally weak (*SI Appendix, Table S9*), and distribution of the signal across the phylogeny was not uniform (Fig. 6). A few clades showed little or no statistically significant phylogenetic autocorrelation for any bone microstructure variable (Fig. 6); these clades included monotremes and our sample of mustelids and rodents (Fig. 6). In *Kryoryctes cadburyi*, P (a measure proportional to the size of medullary cavity) showed statistically significant phylogenetic correlation, suggesting that this variable in *Kryoryctes* has been influenced by phylogeny. Overall, however, the results indicate that for monotremes, unlike many mammalian clades, these parameters of humeral bone microstructure are generally not strongly constrained by phylogeny, suggesting they more likely directly reflect ecology.

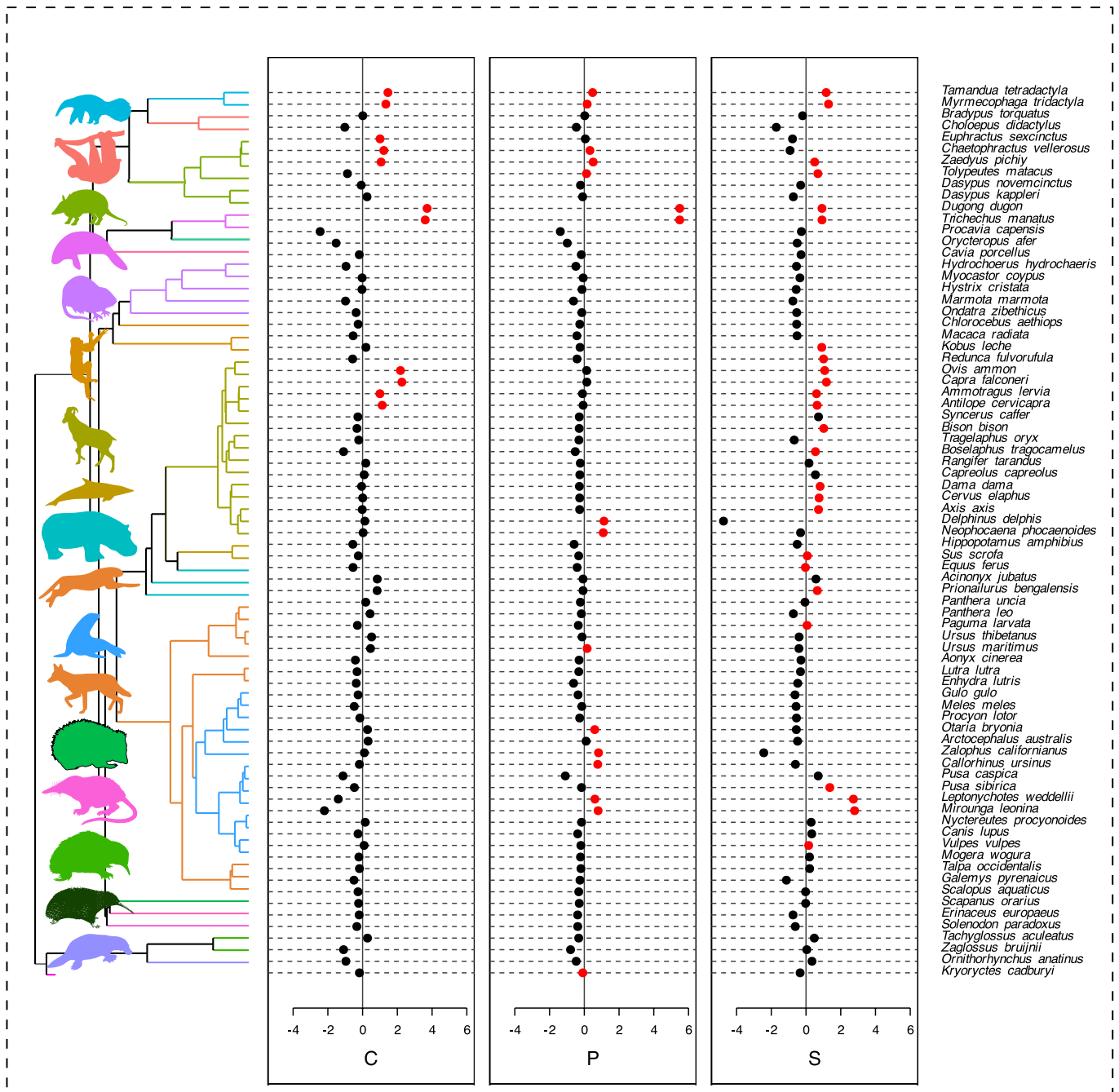


**Fig. 6.** Distribution of phylogenetic signal in bone microstructure across our phylogeny (modified from Upham et al. (16); see *Material and Methods*) estimated by Moran's I index of autocorrelation (see also *SI Appendix*, Fig. S9 and Table S9). Red dots represent statistically significant phylogenetic autocorrelation. Monotremes show no phylogenetic signal in bone microstructure variables, with the exception of P in *Kryoryctes cadburyi*. Mammal silhouettes from PhyloPic.

## Discussion

The qualitative and quantitative analyses of humeral morphology and the phylogenetic analysis presented here all suggest that *K. cadburyi* is a stem-monotreme, as has been previously suggested (27, 35). We found the short, broad humerus of monotremes to be apomorphic for the clade, with similarities to archaic synapsids and some nonmammaliaform cynodonts evidently resulting from evolutionary convergence rather than retention of a plesiomorphic synapsid condition (see also ref. 40). The specialized monotreme humerus occupies a unique morphofunctional space among extant and extinct synapsids (40, 54, 55), distinguished by high humeral torsion, muscle leverage for long-axis rotation, and bending strength (40), which is reflected in the unusual but

energetically efficient way platypuses swim (56) although not efficiently walk (57).

Among extant monotremes, the *Kryoryctes* humerus is closest in external morphology to the terrestrial echidnas, and in particular *Zaglossus* species (Fig. 2 and *SI Appendix*, Fig. S4). However, its microstructure is unlike that of echidnas, which have very thin bone walls, and also diverges from that of most terrestrial mammals, which typically have long bones with a thin/simple tubular structure (43, 51, 58) (*SI Appendix*, Fig. S6 Q–Y).

Instead, the *Kryoryctes* humerus exhibits microstructural features that are characteristic of extant semiaquatic mammals, such as the platypus, including a particularly thick cortex (bone wall) and a very reduced medulla (bone cavity) (51, 58). These features result in markedly increased bone mass, which is known to increase

ballast and help decrease buoyancy in extant semiaquatic (e.g., sea otter, platypus) and exclusively aquatic but slow, shallow-diving mammals (e.g., dugong) (59, 60). This osteosclerosis makes long bones relatively heavy and less resistant to fracture (61), and locomotion on land energetically expensive (57, 62). Hence, this specialization is rarely found in amniotes that move efficiently on land (51, 60, 63–65), exceptionally occurring in large, graviportal mammals (>1 tonne) such as rhinoceroses and hippopotamoids (*SI Appendix, Fig. S6J*), in which increased bone mass assists with body support and propulsion (60, 66). It also occurs in some small subterranean mammals such as naked mole rats (67) and some talpids (44, 45, 68), in which the bone wall is thick but the medullary cavity remains relatively free of trabeculae (*SI Appendix, Fig. S6 BB and CC*), unlike the condition in aquatic mammals, whose bones are subjected to greater multidirectional stresses than those in the gravity-dominated terrestrial environment (see also below).

Among aquatic mammals, markedly increased bone mass is most prevalent in amphibious, shallow-diving and bottom-walking taxa (e.g., coypu, dugong; *SI Appendix, Fig. S6 E and F*), and not in fast-swimming, highly maneuverable, or deep-water predators (e.g. dolphins, seals; *SI Appendix, Fig. S6 A–D*), which instead exhibit a spongy inner organization for a more homogenous distribution of mechanical stresses (49). The cross- and longitudinal sections of inner bone structure in the *Kryoryctes* humerus are both very similar to those of the semiaquatic sea otter *Enhydra lutris* (58) (*SI Appendix, Fig. S6N*), and to a lesser extent to those of some fossil whales, such as the protocetids *Qaisracetus arifi* (whose humerus has a thicker cortex and less compacted trabecular network) and *Maiacetus inuus* [in which the cortex is relatively thinner and trabecular network more homogeneous around the growth center (65); *SI Appendix, Fig. S7 K–M*]. The sea otter *Enhydra* spends almost all of its time in the ocean and is very clumsy on land, which is congruent with the very strong osteosclerosis observed in its femur (58). Other extant otters, which are agile on land, show a lower degree of cortical thickening (58) than does *Kryoryctes*. Based only on the humerus, the inner bone structure of *Kryoryctes* is consistent with it using both aquatic and terrestrial locomotion, as in extant semiaquatic burrowers such as muskrat, river otter, clawless otter, coypu, and platypus. Its femur, if found, could provide further clues as to how much time *Kryoryctes* might have spent on land. Additional functional inferences about fossil forms like *Kryoryctes* should be possible as the development of microtomography increases availability of longitudinal sections of long bones in extant semiaquatic and fossorial species. This will enable a more comprehensive comparison of whole bone microstructure than can be obtained from cross-sections alone, an approach necessitated to date. Coupled with biomechanical analyses, it should help to better distinguish between these two specializations as reflected in fossil bones.

Nonmammaliaform synapsids are absent from the Australian Mesozoic record, with Australia's Cretaceous synapsid faunas instead being dominated by monotremes and monotreme relatives (2, 22, 25, 33, 69). Our phylogenetic analysis suggests that similarities in humeral shape between *Kryoryctes* and some nonmammaliaform synapsids and early mammaliaforms (e.g., *Haldanodon*, *Castorocauda*, *Fruitafossor*) are indicative of morphological convergence in evidently habitually digging and swimming species (39, 70, 71) rather than close relationship (Fig. 1 and *SI Appendix, Fig. S2*; see also ref. 35). This is also likely to be the case for similarities in bone microstructure, such as cortical thickness and medulla form (*SI Appendix, Fig. S7*), between distantly related nonmammaliaform synapsids and early mammaliaforms. As shown by multiple studies documenting marked and evolutionarily rapid shifts throughout the fossil record, bone microanatomy responds

much more quickly to ecological change than does bone shape, especially during adaptation to an aquatic or semiaquatic lifestyle (50, 60).

Based on the evidence available, it is most parsimonious to assume a single origin of a semiaquatic ecomorphotype in the monotreme stem-lineage during the Mesozoic, at some time prior to the age of *Kryoryctes* in the Early Cretaceous, with the ancestor of crown-clade Monotremata retaining this semiaquatic lifestyle (although inferences based on ancestral state reconstructions of bone microstructure cannot rule out a fossorial ancestry for crown monotremes; see above).

In this scenario, the living platypus, *Ornithorhynchus anatinus*, has retained the ancestral monotreme ecomorphology, and the fully terrestrial tachyglossid ecomorphotype is interpreted as having evolved from a semiaquatic ancestor, as has previously been suggested by several authors (7–13). Alternative interpretations – namely that *Kryoryctes* belongs to another synapsid lineage that independently evolved a monotreme-like humeral morphology, or that *Kryoryctes* represents a separate origin of a semiaquatic lifestyle within Monotremata – are possible but less parsimonious.

The timing of the origin of the echidna morphotype remains highly uncertain. The composite 95% highest posterior density interval from clock estimates for the divergence of the platypus and echidna lineages is very broad spanning from the Late Cretaceous to the late Neogene (119 to 7 Ma) (12, 14–21), and derived echidna features could plausibly have arisen long after this initial divergence. *Zaglossus* (or *Megalibgwilia*) *robustus* is known from a clearly echidna-like fossil cranium collected from the Deep Lead mine shaft at Gulgong, New South Wales (72). This deposit, which is now inaccessible, has been suggested to be Early Miocene in age (73), in which case that fossil is by far the oldest known tachyglossid, and provides a minimum age for the evolution of the echidna morphotype. However, it may in fact date to the Pleistocene (2, 5, 74), in which case the Gulgong deposit is similar in age to other Pleistocene deposits containing fossil tachyglossids (e.g., Nelson Bay, Victoria; Naracoorte Caves, South Australia; Darling Downs, Queensland) (2, 75), and so does little to constrain when echidna features originated. It has been proposed that tachyglossids evolved in a geographically isolated region such as the Vogelkop Peninsula of western New Guinea (2), but there is as yet no fossil evidence in support of this hypothesis, and the lack of definitive tachyglossid fossils prior to the Pleistocene may instead reflect the overall highly incomplete record of Australian terrestrial mammals (73). Confident resolution of tachyglossid origins must await future fossil discoveries.

Globally, the vast majority of known Mesozoic mammaliaforms were <1 kg [although multiple exceptions are now known (76–78)], and larger body masses appear to have evolved in relatively few clades, with most known examples from the Southern Hemisphere (79). Although the Australian Mesozoic mammaliaform fossil record is poor, the only species with body masses of 1 kg or greater currently known are the steropodontid monotremes *S. galmani*, with a body mass of approximately 2 kg (2, 22), and *Stirtodon elizabethae* (based on tooth size, the largest known monotreme) (80, 81); the opalionid monotreme *Opalios splendens*, with an estimated dentary length of 76 mm suggesting an estimated body mass of ~1 kg, similar to small *Ornithorhynchus anatinus* adults (82, 83); and the kollikodontids *Sundrius ziegleri* and *Kollikodon ritchiei* [both with estimated body masses of 4 to 8 kg (2)], which are probably monotremes or close relatives (2, 26, 81, 83). Indeed, the humerus of *Kryoryctes cadburyi* appears to be an appropriate size for referral to any of these taxa, all of which are known only from dental or cranial remains. It has been suggested (2) that *Kryoryctes cadburyi* may be synonymous with

*S. ziegleri*, which is from a stratigraphically equivalent fossil locality 12 km distant.

There have been more than 30 transitions from a fully terrestrial lifestyle to a semiaquatic or fully aquatic lifestyle among mammaliaforms (62, 70, 84, 85). This includes at least four times among Mesozoic mammaliaforms, namely in docodontans, eutriconodontans, potentially stagodontid marsupialiforms (3, 39, 86), and (as we show here) in monotremes. Among extant mammals, molecular clock analyses (16, 17) suggest that, in contrast to monotremes, all extant aquatic and semiaquatic placental and marsupial lineages originated in the Cenozoic.

Compelling evidence for the reverse transition, back to full terrestriality from an at least partially aquatic ancestry, is rarer. Farina et al. (87) found that evolutionary transitions in mammals between terrestrial and semiaquatic lifestyles have occurred in both directions, but that they become rarer and irreversible in more strictly water-adapted lineages. Evolutionary transitions involving a change from compact cortical bone to more cancellous bone have been recorded in lineages moving from a semiaquatic to a fully aquatic deep diving lifestyle, for example, cetaceans (65, 88) and mosasaurs (89). Similar bone tissue remodeling could have been involved in skeletal lightening during a shift from a semiaquatic to a fully terrestrial lifestyle, as suggested here for echidnas. Bone inner structure is known to be plastic and to potentially evolve faster than morphology in functional adaptation (90, 91). In echidnas, the cortex of the long bones is extremely thin relative to that in other burrowing mammals, and more analogous to juvenile placental mammals (92), highlighting the similarity in bone microstructure of *Kryoryctes* to the platypus rather than echidnas and suggesting a pronounced ecomorphological shift away from a less derived, platypus-like form.

When *Kryoryctes* lived, during the Early Cretaceous, Dinosaur Cove lay within the Antarctic Circle, at ~70°S (36, 42). This high-latitude position implies prolonged periods of complete winter darkness (34, 93, 94) despite a relatively mild, wet, cool-to-warm-temperate climate (34, 95–97). The extant semiaquatic platypus famously uses electro- and mechanoreceptors on the bill to locate its freshwater prey, irrespective of available light (4), and tachyglossids retain similar but less numerous receptors on the beak (11), though how these are used for foraging is unclear (5). Electro- or mechanosensitivity would represent an important adaptation or exaptation for southern polar life in *Kryoryctes* and other stem monotremes or relatives such as Lightning Ridge's *S. galmani* and *K. ritchiei*, which also lived within the Cretaceous Antarctic Circle (98) and which may also have been semiaquatic (2, 22, 26, 83).

Monotremes are one of few nontherian Southern Hemisphere mammal groups that are known to have survived the K-Pg event (99), and the only one of these to persist to the present day. The Southern Hemisphere terrestrial vertebrate fauna may have been less severely affected by the K-Pg extinction event than that of North America, perhaps because it was much further away from the Yucatan bolide impact (100, 101). However, the event had a global impact, resulting in the total extinction of several terrestrial vertebrate groups (e.g., nonavian dinosaurs, pterosaurs) (102). The survival of stem monotremes across the K-Pg boundary may also have been connected to their long-held semiaquatic habits. Chemical buffering is thought to have reduced the effects of a significant period of acid rain for freshwater animals (e.g., crocodiles, turtles, frogs, fish) not afforded to terrestrial mammals, which were significantly affected (av. 10% diversity loss for freshwater species versus 50%-plus loss for terrestrial) (103, 104). Thermal refugia were also critical for survival (104) and, as

semiaquatic burrowers, monotremes may have been able to shelter in bank-side burrows during the ecological disruption that marked the end of the Cretaceous. For mammals that could also use torpor and other heterothermies to endure resource shortages (105, 106), and electroreception to facilitate opportunistic, around-the-clock foraging during long periods of darkness (4, 107), the outcomes immediately following the K-Pg event may have been less catastrophic for stem monotremes than for strictly terrestrial species.

## Materials and Methods

**Materials.** The holotype of *K. cadburyi* is an incomplete right humerus (NMV P208094) recovered from the Early Cretaceous [early to middle Albian, 108 to 103 Ma (34)] Eumeralla Formation at Slippery Rock Site, Dinosaur Cove, southern Victoria, Australia (82) (Fig. 1). A fragmentary premolar (NMV P208383) was found within 6 m of the holotype (33), and may represent *K. cadburyi* (2). Previous detailed qualitative comparisons (35) of NMV P208094 with the humeri of extinct and extant mammaliaforms suggested that it is most similar overall to monotremes, and, among them, closest in morphology and size to *Tachyglossus*, but that it lacks derived features of the humerus shared by the extant platypus and echidnas (e.g., absence of olecranon fossa, oblique orientation of the epicondylar axis with respect to the long axis of the humerus, laterally shifted position of the humeral contribution to the elbow joint, and bulbous, combined condyle for the radius and ulna).

The gross morphology of NMV P208094 was compared with a range of extant terrestrial, semiaquatic, and fossorial mammals, and with Mesozoic mammaliaforms for which humeral morphology is known, based on direct examination of specimens (where available), or published figures and descriptions (*SI Appendix*).

**Data Acquisition.** To allow quantitative comparison of 3D shape and microstructure analysis, NMV P208094 and the humeri of the following extant monotremes were microCT-scanned: *O. anatinus* (NMV C11285, UNSW AR22920, UNSW AR22921), short-beaked echidna *T. aculeatus* (NMV C2562, UNSW AR22922, UNSW AR5990); western long-beaked echidna *Z. bruijnii* (NMV C11586) (*SI Appendix, Table S4*). NMV refers to Museum Victoria, Melbourne, and UNSW AR refers to the UNSW Sydney Vertebrate Palaeontology Collections, respectively. Specimens were collected under permit or donated by zoos to those institutions. All appear to represent adult specimens in which epiphyses are fused to the diaphysis, as they appear to be in the humerus of *K. cadburyi*. Specimens were scanned using an Xradia MicroXCT scanner at Monash University, Melbourne, or a Siemens Inveon MicroPET-CT scanner at UNSW Sydney, DINGO thermal-neutron imaging instrument at ANSTO, Sydney, and Thermo Fisher Scientific HeliScan II at UNSW Sydney. Image segmentation, visualization, and measuring was performed using Inveon Research Workplace 4.2 (Siemens), Avizo 9 (Thermo Fisher Scientific), Mimics 20.0 (Materialise), VGSTUDIO MAX version 2.2 (Volume Graphics Inc.), and Rhinoceros 5 (Robert McNeel & Associates, Seattle, WA). For the *Kryoryctes cadburyi* humerus (NMV P208094), imaging obtained from microCT and thermal-neutron scan datasets was similar. Neutron tomography provided slightly improved contrast relative to microCT tomography (*SI Appendix, Fig. S10*), but we used the microCT dataset for our analyses because of its slightly higher spatial resolution.

**Data Analysis.** To assess its likely phylogenetic affinities, *K. cadburyi* was added to a large taxon-character matrix of 71 mammal and mammaliaform ingroup taxa and six nonmammaliaform cynodont outgroup taxa and 536 morphological characters modified from Huttenlocker et al. (38), with modifications to character scorings based on Woodburne et al. (108), Rougier et al. (109), Rowe et al. (24), Phillips et al. (12), Pian et al. (26), and our own observations (*Dataset S1*). This matrix is restricted to taxa known from humeral remains, to ensure that at least some scored characters overlap between *Kryoryctes* and the other taxa. *Kryoryctes* could be scored for 17 out of 536 morphological characters, rendering it 3.2% complete.

In the final matrix, 512 characters were parsimony informative, and 105 characters representing plausible morphoclines were specified as ordered. The matrix was analyzed using maximum parsimony (MP) in TNT v1.5 (110), starting with an initial "New Technology" search (with sectorial search, ratchet, drift, and tree fusing) that was run until the same minimum length was found 100 times,

followed by a "Traditional" search (with tree bisection reconnection) within the trees found by the initial search. The most parsimonious trees were then summarized using strict consensus. Support for nodes present in the strict consensus was calculated using 2000 standard bootstrap replicates with traditional search, and with results output as absolute frequencies. Synapomorphies for specific clades were identified by optimizing the taxon-character matrix on the strict consensus topology using maximum parsimony, as implemented by the "Trace Character History" option in Mesquite v3.81 (111).

Virtual comparisons of 3D digital models were used to infer the interpreted orientation of the humerus of *Kryoryctes*, and its overall similarity to its inferred closest living relatives, the extant monotremes *O. anatinus*, *T. aculeatus*, and *Z. bruijini* (SI 3D models <https://figshare.com/s/c6e0a6909a2462dddb11>) (37). Virtual comparisons were conducted in Rhinoceros 5. The principal axis of inertia was automatically calculated for each of the four models separately and used to align each model to the world coordinate system. Each model was then rotated about the principal axis to provide a gross alignment of shape. Visual comparison was aided by calculation of mesh-mesh deviation in Rhinoceros 5 using the AdvMesh v.0.2 open source plug-in (112). Mesh-mesh deviation is a projection of the distances, coded by color, calculated between the vertices on one mesh (reference mesh) relative to the other (evaluate mesh) and provides a heat map visualization of gross similarity/difference. In each case, *Kryoryctes* was used as the evaluate mesh (i.e., evaluated relative to each species).

Virtual sections of our scanned humeri of *Kryoryctes*, *Ornithorhynchus*, *Tachyglossus*, and *Zaglossus* were made as follows: Longitudinal sections were made in the coronal plane (in dorsal view) and in the sagittal plane (90° to coronal section) at approximately mid-diaphysis, and cross-sections at the inferred center of ossification (as determined by the longitudinal sections). The cross-sections were transformed into binary images following Laurin et al. (52) and using Adobe Creative Cloud. Bone was designated as black, and all other surfaces (medullary cavity, resorption areas, and vascular spaces) as white (Fig. 3 A–D and SI Appendix, Fig. S5). Bone density distribution in the mid-diaphyseal reference section was calculated (independent of the operator) by the software Bone Profiler (43) and using the settings of ontogenetic center, 60 angles and 100 distances, for the following parameters: C, global bone compactness for the sectional area; P, relative distance from center of the section to point of inflection, where the most abrupt change in compactness is observed, and is proportional to size of medullary cavity; S, reciprocal of the slope at inflection point, generally reflecting width of the transition zone between cortical bone and medullary region. The bone microstructure parameters C, S, and P have been shown to be correlated with ecology in numerous studies of tetrapods (e.g., refs. 43, 44, 52, 59, 68, and 113). Values of C, P, and S for the humeri of *Kryoryctes*, *Ornithorhynchus*, *Tachyglossus*, and *Zaglossus* were calculated and added to those given by Hayashi et al. (table 3 of ref. 49), Straehl et al. (table S2.1 of ref. 113), Meier et al. (appendix 2 of ref. 68), and Derbridge et al. (114) for a total of 82 living mammals of known habit (SI Appendix, Table S4). We used the habit categories of Hayashi et al. (49): terrestrial (T), fossorial (F), exclusively aquatic poorly active swimmers (PA), essentially or exclusively aquatic deep divers (D), but split their semiaquatic shallow swimmers or divers category into semiaquatic burrowers (bSA: species of *Ornithorhynchus*, *Ondatra*, *Myocastor*, *Lutra*, *Aonyx*) and semiaquatic nonburrowers (SA) (SI Appendix, Table S4). In these analyses, we restricted our comparative taxa to living species in order to avoid inferring a lifestyle for *Kryoryctes* based partly on hypotheses about the habits of extinct species [viz. Myhrvold et al. (115)].

R packages *stats* and *MASS* in R version 3.6 were used to conduct a Principal Component Analysis and linear discriminant analyses (LDA) using values of C, P, and S to infer the lifestyle of *Kryoryctes* based on comparative taxa of known ecology. pFDA offers an alternative to LDA, however displays some problematic characteristics (116), and was not used because we wished to infer the likely ancestral habit for Monotremata. Boxplots were used to compare C, P, and S values in the *Kryoryctes* humerus with those of extant mammals in six habit categories (T, F, D, PA, SA, bSA). Dunnett's pairwise comparisons of the means of C, P, and S were used to test for statistical significance between these traits in the different ecologies. We used *StableTraits* (117) to reconstruct the states for C, P, and S in the MRCA of monotremes, and included these values in an LDA to infer the likely ancestral habit for Monotremata. Phylogenetic tree building for the 82 extant species dataset was done by pruning Upham et al.'s (16) composite species-level mammal phylogeny. *Kryoryctes* was then added as sister to Monotremata (congruent with our phylogenetic results; Fig. 1); five different trees were prepared, each with a different branch length leading to *Kryoryctes* (0.001, 1, 5, 10, 20 Ma), with the timing of divergence from Monotremata specified in each tree so that the tip age of *Kryoryctes* was 106 Ma. Moran's I index of autocorrelation was used to estimate the distribution of phylogenetic signal across the phylogeny.

**Data, Materials, and Software Availability.** 3D models data have been deposited in figshare (<https://figshare.com/s/c6e0a6909a2462dddb11>) (37). All other data are included in the manuscript and/or supporting information.

**ACKNOWLEDGMENTS.** This research was supported by Australian Research Council grants DP180100792 (S.J.H., M.A., and R.M.D.B.), DE150100862 and FT200100822 (L.A.B.W.), and DP230100613 (A.R.E.), ANSTO grant P7905 for access to DINGO, a National Collaborative Research Infrastructure Strategy (NCRIS) capability, at the Australian Centre for Neutron Scattering, ANSTO, and the Tyree X-ray Micro-CT and Biological Resources Imaging Laboratories in the Mark Wainwright Analytic Centre at UNSW Sydney, a node of the National Imaging Facility. The phylogenetic analysis program TNT is made available with the sponsorship of the Willi Hennig Society. S. Regnault and S. Pierce provided humeral measurements for *Tachyglossus aculeatus* specimens. Brian Davis provided access to undescribed material of *Fruitafossor windsheffeli*. We thank G. Rougier, B. Davis, and C. Kammerer for very helpful discussion, and our editor Z.-X. Luo and reviewers L. N. Weaver, R. W. Blob, and M. R. Whitney whose criticisms and insights significantly improved our manuscript.

Author affiliations: <sup>a</sup>School of Biological, Earth and Environmental Sciences, The University of New South Wales, Sydney, NSW 2052, Australia; <sup>b</sup>School of Archaeology and Anthropology, College of Arts and Social Sciences, The Australian National University, Canberra, ACT 2601, Australia; <sup>c</sup>Australian Research Council Training Centre for Multiscale 3D Imaging, Modelling and Manufacturing, Research School of Physics, The Australian National University, Canberra, ACT 2601, Australia; <sup>d</sup>Department of Anthropology, University of Toronto Scarborough, Scarborough, ON M1C 1A4, Canada; <sup>e</sup>Museo de La Salle, Universidad de La Salle, Bogotá 111711, Colombia; <sup>f</sup>Escuela de Biología, Universidad Industrial de Santander, Bucaramanga 680003, Colombia; <sup>g</sup>UMR 7179 Mécanismes adaptatifs et Évolution, Centre National de la Recherche Scientifique, Muséum National d'Histoire Naturelle, Paris 75005, France; <sup>h</sup>Australian Centre for Neutron Scattering, Australian Nuclear Science and Technology Organisation, Lucas Heights, NSW 2234, Australia; <sup>i</sup>School of Biological Sciences, Monash University, Melbourne, VIC 3800, Australia; <sup>j</sup>Museums Victoria Research Institute, Museums Victoria, Melbourne, VIC 3001, Australia; <sup>k</sup>Tyree X-ray Micro-Computed Tomography Laboratory, Mark Wainwright Analytical Centre, The University of New South Wales, Sydney, NSW 2052, Australia; <sup>l</sup>Biological Resources Imaging Laboratory, Mark Wainwright Analytical Centre, The University of New South Wales, Sydney, NSW 2052, Australia; <sup>m</sup>School of Earth, Atmosphere and Environment, Monash University, Melbourne, VIC 3800, Australia; and <sup>n</sup>School of Science, Engineering, and Environment, University of Salford, Manchester M5 4WT, United Kingdom

- C. J. Burgin, J. P. Colella, P. L. Kahn, N. S. Upham, How many species of mammals are there? *J. Mammal.* **99**, 1–14 (2018).
- T. F. Flannery et al., A review of monotreme (Monotremata) evolution. *Alcheringa* **45**, 1–18 (2022).
- Z. Kielan-Jaworowska, R. L. Cifelli, Z.-X. Luo, *Mammals from the Age of Dinosaurs: Origins, Evolution, and Structure* (Columbia University Press, 2004).
- T. Grant, *Platypus* (CSIRO Publishing, 2007).
- M. L. Augee, B. Gooden, A. M. Musser, *Echidna: Extraordinary Egg-Laying Mammal* (CSIRO Publishing, 2006).
- I. J. Menzies, *Handbook of New Guinea Marsupials and Monotremes* (Kristen Press, 1991).
- W. K. Gregory, Monotremes and the palimpsest theory. *Bull. Am. Mus. Nat. Hist.* **88**, 1–52 (1947).
- W. K. Gregory, *Evolution Emerging, A Survey of Changing Patterns from Primeval Life to Man* (The MacMillan Company, 1957), vol. 1.
- R. Pascual et al., "The first non-Australian monotreme: An early Paleocene South American platypus (Monotremata, Ornithorhynchidae)" in *Platypus and Echidnas*, M. Augee, Ed. (Royal Zoological Society of New South Wales, 1992), pp. 1–14.
- M. Archer, P. Murray, S. J. Hand, H. Godthelp, "Reconsideration of monotreme relationships based on the skull and dentition of the Miocene *Obdurodon dicksoni*" in *Mammal Phylogeny: Mesozoic Differentiation, Multituberculates, Monotremes, Early Therians, and Marsupials*, F. S. Szalay, M. J. Novacek, M. C. McKenna, Eds. (Springer-Verlag, 1993), pp. 75–94.
- J. D. Pettigrew, Electrosensory reception in monotremes. *J. Exp. Biol.* **202**, 1447–1454 (1999).
- M. J. Phillips, T. H. Bennett, M. S. Y. Lee, Molecules, morphology, and ecology indicate a recent, amphibious ancestry for echidnas. *Proc. Natl. Acad. Sci. U.S.A.* **106**, 17089–17094 (2009).
- S. Mirceta et al., Evolution of mammalian diving capacity traced by myoglobin net surface charge. *Science* **340**, 1234192 (2013).
- R. W. Meredith et al., Impacts of the Cretaceous Terrestrial Revolution and KPg extinction on mammal diversification. *Science* **334**, 521–524 (2011).
- M. J. Phillips, Four mammal fossil calibrations: Balancing competing palaeontological and molecular considerations. *Palaeontol. Electron.* **18**, 1–16 (2015).
- N. S. Upham, J. A. Esselstyn, W. Jetz, Inferring the mammal tree: Species-level sets of phylogenies for questions in ecology, evolution, and conservation. *PLoS Biol.* **17**, e3000494 (2019).

17. S. Álvarez-Carretero *et al.*, A species-level timeline of mammal evolution integrating phylogenomic data. *Nature* **602**, 263–267 (2021).
18. Y. Zhou *et al.*, Platybus and echidna genomes reveal mammalian biology and evolution. *Nature* **592**, 756–762 (2021).
19. J. Wang *et al.*, A monotreme-like auditory apparatus in a Middle Jurassic haramiyidan. *Nature* **590**, 279–283 (2021).
20. Z. Yu *et al.*, Temporal framework for the Yanliao Biota and timing of the origin of crown mammals. *Earth Planet. Sci. Lett.* **617**, 118246 (2023).
21. F. Mao *et al.*, Jurassic shuotheriids show earliest dental diversification of mammaliaforms. *Nature* **628**, 569–575 (2024).
22. M. Archer, T. F. Flannery, A. Ritchie, R. E. Molnar, First Mesozoic mammal from Australia—an early Cretaceous monotreme. *Nature* **318**, 363–366 (1985).
23. T. H. Rich *et al.*, Early Cretaceous mammals from Flat Rocks, Victoria, Australia. *Rec. Queen Victoria Mus.* **106**, 1–35 (1999).
24. T. Rowe, T. H. Rich, P. Vickers-Rich, M. Springer, M. O. Woodburne, The oldest platypus and its bearing on divergence timing of the platypus and echidna clades. *Proc. Natl. Acad. Sci. U.S.A.* **105**, 1238–1242 (2008).
25. T. H. Rich *et al.*, The mandible and dentition of the Early Cretaceous monotreme *Teinolophos trusleri*. *Alcheringa* **40**, 475–501 (2016).
26. R. Pian, M. Archer, S. J. Hand, R. M. D. Beck, A. Cody, The upper dentition and relationships of the enigmatic Australian Cretaceous mammal *Kollikodon ritchiei*. *Mem. Mus. Vic.* **74**, 97–105 (2016).
27. M. A. Celik, M. J. Phillips, Conflict resolution for Mesozoic mammals: Reconciling phylogenetic incongruence among anatomical regions. *Front. Genet.* **11**, 0651 (2020).
28. B. King, R. M. D. Beck, Tip dating supports novel resolutions of controversial relationships among early mammals. *Proc. R. Soc. Lond. B Biol. Sci.* **287**, 20200943 (2020).
29. J. T. Wilson, On the skeleton of the snout of the mammary foetus of monotremes. *Proc. Linn. Soc. N.S.W.* **26**, 717–737 (1901).
30. A. M. Musser, M. Archer, New information about the skull and dentary of the Miocene platypus *Obdurodon dicksoni* and a discussion of ornithorhynchid relationships. *Philos. Trans. R. Soc. Lond. B Biol. Sci.* **353**, 1063–1079 (1998).
31. A. B. Camens, Were early Tertiary monotremes really all aquatic? Inferring palaeobiology and phylogeny from a depauperate fossil record. *Proc. Natl. Acad. Sci. U.S.A.* **107**, E12 (2009).
32. K. W. S. Ashwell, "Reflections: Monotreme neurobiology in context" in *Neurobiology of Monotremes: Brain Evolution in Our Distant Mammalian Cousins*, K. W. S. Ashwell, Ed. (CSIRO Publishing, 2013), pp. 285–298.
33. T. H. Rich, P. Vickers-Rich, Diversity of Early Cretaceous mammals from Victoria, Australia. *Bull. Am. Mus. Nat. Hist.* **285**, 36–53 (2004).
34. S. F. Poropat *et al.*, Early Cretaceous polar biotas of Victoria, southeastern Australia—An overview of research to date. *Alcheringa* **42**, 157–229 (2018).
35. P. A. Pridmore, T. H. Rich, P. Vickers-Rich, P. P. Gambaryan, A tachyglossid-like humerus from the Early Cretaceous of south-eastern Australia. *J. Mammal. Evol.* **12**, 359–378 (2005).
36. R. D. Müller *et al.*, GPlates: Building a virtual Earth through deep time. *Geochim. Geophys. Geosyst.* **19**, 2243–2261 (2018).
37. S. J. Hand *et al.*, 3D digital models of monotreme humeri. Figshare. <https://figshare.com/s/c6e0a6f09a2462dadb11>. Deposited 20 November 2024.
38. A. K. Huttenlocker, D. M. Grossnickle, J. I. Kirkland, J. A. Schultz, Z.-X. Luo, Late-surviving stem mammal links the lowermost Cretaceous of North America and Gondwana. *Nature* **558**, 109–112 (2018).
39. T. Martin, Postcranial anatomy of *Haldanodon exspectatus* (Mammalia, Docodonta) from the Late Jurassic (Kimmeridgian) of Portugal and its bearing for mammalian evolution. *Zool. J. Linn. Soc.* **145**, 219–248 (2005).
40. R. J. Brocklehurst, M. Mercado, K. D. Angielczyk, S. E. Pierce, Adaptive landscapes unveil the complex evolutionary path to mammalian forelimb function and posture. *bioRxiv* [Preprint] (2024), <https://doi.org/10.1101/2024.03.12.584484> (Accessed 6 October 2024).
41. C. F. Kammerer, K. D. Angielczyk, J. Fröbisch, Eds., *The Early Evolutionary History of the Synapsida* (Springer, 2014).
42. P. D. Rismiller, F. Grutzner, *Tachyglossus aculeatus* (Monotremata: Tachyglossidae). *Mamm. Species* **51**, 75–91 (2019).
43. M. Girondot, M. Laurin, Bone profiler: A tool to quantify, model and statistically compare bone section compactness profiles. *J. Verteb. Paleontol.* **23**, 458–461 (2003).
44. M. Laurin, A. Canoville, D. Germain, Bone microanatomy and lifestyle: A descriptive approach. *C. R. Palevol.* **10**, 381–402 (2011).
45. J. Gönét, J. Bardin, M. Girondot, J. R. Hutchinson, M. Laurin, Unravelling the postural diversity of mammals: Contribution of humeral cross-sections to palaeobiological inferences. *J. Mammal. Evol.* **30**, 1–17 (2023).
46. A. Chinsamy, J. H. Hurum, Bone microstructure and growth patterns of early mammals. *Acta Palaeontol. Pol.* **51**, 325–338 (2006).
47. D. H. Enlow, S. O. Brown, A comparative histological study of fossil and recent bone tissue. Part 3. *Tex. J. Sci.* **10**, 187–230 (1958).
48. V. de Buffrénil, A. Canoville, R. D'Anastasio, D. P. Domning, Evolution of sirenian pachyostosis, a model case for the study of bone structure in aquatic tetrapods. *J. Mamm. Evol.* **17**, 101–120 (2010).
49. S. Hayashi *et al.*, Bone inner structure suggests increasing aquatic adaptations in *Desmostylia* (Mammalia, Afrotheria). *PLoS One* **8**, e59146 (2013).
50. E. Amson, C. de Muizon, M. Laurin, C. Argot, V. de Buffrénil, Gradual adaptation of bone structure to aquatic lifestyle in extinct sloths from Peru. *Proc. Biol. Sci.* **281**, 20140192 (2014).
51. A. Canoville, M. Laurin, Evolution of humeral microanatomy and lifestyle in amniotes, and some comments on palaeobiological inferences. *Biol. J. Linn. Soc. Lond.* **100**, 384–406 (2010).
52. M. Laurin, M. Girondot, M.-M. Loth, The evolution of long bone microanatomy and lifestyle in lissamphibians. *Paleobiology* **30**, 589–613 (2004).
53. R. W. Blob, "Scaling of the hind limb skeleton in cynognathian cynodonts: Implications for ontogeny and the evolution of mammalian endothermy" in *Amniote Paleobiology: Perspectives on the Evolution of Mammals, Birds, and Reptiles*, M. Carrano, T. Gaudin, R. Blob, J. Wible, Eds. (University of Chicago Press, 2006), pp. 410–428.
54. F. A. Jenkins Jr., The postcranial skeleton of African cynodonts: Problems in the early evolution of the mammalian postcranial skeleton. *Yale Univ. Peabody Mus. Nat. Hist. Bull.* **36**, 1–216 (1971).
55. P. A. Pridmore, Terrestrial locomotion in monotremes (Mammalia: Monotremata). *J. Zool.* **205**, 53–73 (1985).
56. F. E. Fish, R. V. Baudinette, P. B. Frappell, M. P. Sarre, Energetics of swimming by the platypus *Ornithorhynchus anatinus*: Metabolic effort associated with rowing. *J. Exp. Biol.* **200**, 2647–2652 (1997).
57. F. E. Fish, P. B. Frappell, R. V. Baudinette, P. M. MacFarlane, Energetics of terrestrial locomotion of the platypus *Ornithorhynchus anatinus*. *J. Exp. Biol.* **204**, 797–803 (2001).
58. A. Houssaye, L. Botton-Divet, From land to water: Evolutionary changes in long bone microanatomy of otters (Mammalia: Mustelidae). *Biol. J. Linn. Soc. Lond.* **125**, 240–249 (2018).
59. A. Ricqlès, V. de Buffrénil, "Bone histology, heterochronies and the return of tetrapods to life in water: W[h]ere are we?" in *Secondary Adaptation of Tetrapods to Life in Water*, J. M. Mazin, V. de Buffrénil, Eds. (Verlag Dr. Friedrich Pfeil, 2001), pp. 289–310.
60. A. Houssaye, P. M. Sander, N. Klein, Adaptive patterns in aquatic amniote bone microanatomy—more complex than previously thought. *Integr. Comp. Biol.* **56**, 1349–1369 (2016).
61. J. Yan, K. B. Clifton, M. M. Mecholsky, R. L. Reep, Fracture toughness of manatee rib and bovine femur using a chevron-notched beam test. *J. Biomech.* **39**, 1066–1074 (2006).
62. F. E. Fish, Biomechanics and energetics in aquatic and semiaquatic mammals: Platypus to whale. *Physiol. Biochem. Zool.* **73**, 683–698 (2000).
63. A. Houssaye, "Pachyostosis" in aquatic amniotes: A review. *Integr. Zool.* **4**, 325–340 (2009).
64. A. Houssaye, Bone histology of aquatic reptiles: What does it tell us about secondary adaptation to an aquatic life. *Biol. J. Linn. Soc.* **108**, 3–21 (2013).
65. A. Houssaye, P. Tafforeau, C. De Muizon, P. D. Gingerich, Transition of Eocene whales from land to sea: Evidence from bone microstructure. *PLoS One* **10**, e0118409 (2015).
66. A. Houssaye, F. Martin, J.-R. Boisserie, F. Lihoreau, Paleoeological inferences from long bone microanatomical specializations in Hippopotamoidea (Mammalia, Artiodactyla). *J. Mamm. Evol.* **28**, 847–870 (2021).
67. G. Montoya-Sanhueza, A. Chinsamy, Long bone histology of the subterranean rodent *Bathyergus suillus* (Bathyergidae): Ontogenetic pattern of cortical bone thickening. *J. Anat.* **230**, 203–233 (2017).
68. P. S. Meier *et al.*, Evolution of bone compactness in extant and extinct moles (Talpidae): Exploring humeral microstructure in small fossorial mammals. *BMC Evol. Biol.* **13**, 55 (2013).
69. T. F. Flannery *et al.*, A diverse assemblage of monotremes (Monotremata) from the Cenomanian Lightning Ridge fauna of New South Wales, Australia. *Alcheringa* **48**, 319–337 (2024).
70. Q. Ji, Z.-X. Luo, C.-X. Yuan, A. R. Tabrum, A swimming mammaliaform from the Middle Jurassic and ecomorphological diversification of early mammals. *Science* **311**, 1123–1127 (2006).
71. Z.-X. Luo, J. R. Wible, A Late Jurassic digging mammal and early mammalian diversification. *Science* **308**, 103–107 (2005).
72. M. Griffiths, R. T. Wells, D. J. Barrie, Observations on the skulls of fossil and extant echidnas (Monotremata: Tachyglossidae). *Aust. Mammal.* **14**, 87–101 (1991).
73. M. O. Woodburne *et al.*, Biochronology of the continental mammal record of Australia and New Guinea. *Spec. Publ. Sth. Aust. Depart. Mines Energy* **5**, 347–363 (1985).
74. A. M. Musser, "Classification and evolution of the monotremes" in *Neurobiology of Monotremes: Brain Evolution in Our Distant Mammalian Cousins*, K. W. S. Ashwell, Ed. (CSIRO Publishing, 2013), pp. 1–16.
75. J. Long, M. Archer, T. F. Flannery, S. J. Hand, *Prehistoric Mammals of Australia and New Guinea* (UNSW Press, 2002).
76. F. A. Smith *et al.*, The evolution of maximum body size of terrestrial mammals. *Science* **330**, 1216–1219 (2010).
77. G. J. Slater, Phylogenetic evidence for a shift in the mode of mammalian body size evolution at the Cretaceous–Palaeogene boundary. *Methods Ecol. Evol.* **4**, 734–744 (2013).
78. O. Bertrand, Brawn before brains in placental mammals after the end-Cretaceous extinction. *Science* **376**, 80–85 (2022).
79. D. W. Krause *et al.*, Introduction to *Adalatherium hui* (Gondwanatheria, Mammalia) from the Late Cretaceous of Madagascar. *J. Vertebr. Paleontol.* **40** (suppl. 1), 4–18 (2020).
80. W. A. Clemens, G. P. Wilson, R. E. Molnar, An enigmatic (synapsid?) tooth from the Early Cretaceous of New South Wales, Australia. *J. Vertebr. Paleontol.* **23**, 232–237 (2003).
81. T. H. Rich, T. F. Flannery, P. Vickers-Rich, "Evidence for a remarkably large toothed monotreme from the Early Cretaceous of Lightning Ridge, NSW, Australia" in *Biological Consequences of Plate Tectonics: New Perspectives on Post-Gondwana and Break-up*, G. V. Prasad, R. Patnaik, Eds. (Springer International, 2020), pp. 77–81.
82. J. R. Foster, Preliminary mass estimates for mammalian genera of the Morrison formation (Upper Jurassic; North America). *Paleobios* **28**, 114–122 (2009).
83. T. F. Flannery, M. Archer, T. H. Rich, R. Jones, A new family of monotremes from the Cretaceous of Australia. *Nature* **377**, 418–420 (1995).
84. A. Berta, "Pinniped evolution" in *Encyclopedia of Marine Mammals*, W. F. Perrin, B. Würsig, J. G. M. Thewissen, Eds. (Academic Press, 2009), pp. 861–868.
85. G. A. Hood, *Semi-Aquatic Mammals: Ecology and Biology* (Johns Hopkins University Press, 2020).
86. M. Chen, G. P. Wilson, A multivariate approach to infer locomotor modes in Mesozoic mammals. *Paleobiology* **41**, 280–312 (2015).
87. B. M. Farina, S. Faurby, D. Silvestro, Dollo meets Bergmann: Morphological evolution in secondary aquatic mammals. *Proc. R. Soc. B* **290**, 20231099 (2023).
88. N.-M. Gray, K. Kainec, S. Madar, L. Tomko, S. Wolfe, Sink or swim? Bone density as a mechanism for buoyancy control in early cetaceans. *Anat. Rec.* **290**, 638–653 (2007).
89. A. Houssaye *et al.*, Microanatomical and histological features in the long bones of mosasaurine mosasaurs (Reptilia, Squamata)—implications for aquatic adaptation and growth rates. *PLoS One* **8**, e76741 (2013).
90. A. Houssaye, V. de Buffrénil, "Bone histology and the adaptation to aquatic life in tetrapods" in *Vertebrate Skeletal Histology and Paleohistology*, V. de Buffrénil, A. de Ricqlès, L. Zylberberg, K. Padian, Eds. (CRC Press, 2021), pp. 744–754.
91. E. Amson *et al.*, Unique bone microanatomy reveals ancestry of subterranean specializations in mammals. *Evol. Lett.* **6**, 552–561 (2022).
92. L. N. Weaver *et al.*, Multituberculate mammals show evidence of a life history strategy similar to that of placentals, not marsupials. *Amer. Nat.* **200**, 383–400 (2020).
93. T. H. Rich, P. Vickers-Rich, *Dinosaurs of Darkness* (Indiana University Press, 2000).
94. J. L. Kitchener, N. E. Campione, E. T. Smith, P. R. Bell, High-latitude neonate and perinate ornithopods from the mid-Cretaceous of southeastern Australia. *Sci. Rep.* **9**, 19600 (2019).

95. T. H. Rich, P. Vickers-Rich, "Climatic setting of the polar dinosaurs of south-east Australia" in *Windows on Meteorology: Australian Perspectives*, E. K. Webb, Ed. (CSIRO Publishing, 1997), pp. 59–66.
96. A. Constantine, A. Chinsamy, P. Vickers-Rich, T. H. Rich, Periglacial environments and polar dinosaurs. *S. Afr. J. Sci.* **94**, 137–141 (1998).
97. G. J. Retallack, Dinosaur and tree-line invasion of southeastern Australia during Cretaceous greenhouse spikes. *Aust. J. Earth Sci.* **70**, 840–858 (2023).
98. P. R. Bell *et al.*, Revised geology, age, and vertebrate diversity of the dinosaur-bearing Griman Creek Formation (Cenomanian), Lightning Ridge, New South Wales, Australia. *Palaeogeogr. Palaeoclimatol. Palaeoecol.* **514**, 655–671 (2019).
99. G. W. Rougier, A. G. Martinelli, A. M. Forasiepi, *Mesozoic Mammals from South America and Their Forerunners* (Springer Nature, 2021).
100. J. V. Morgan, T. J. Bralower, J. Brugger, K. Wünnemann, The Chicxulub impact and its environmental consequences. *Nat. Rev. Earth Environ.* **3**, 338–354 (2022).
101. P. Wilf, M. R. Carvalho, E. Stiles, The end-Cretaceous plant extinction: Heterogeneity, ecosystem transformation, and insights for the future. *Cambridge Prisms Extinction* **1**, e14 (2023).
102. P. Schulte *et al.*, The Chicxulub asteroid impact and mass extinction at the Cretaceous-Paleogene boundary. *Science* **327**, 1214–1218 (2010).
103. D. S. Robertson, M. C. McKenna, O. B. Toon, S. Hope, J. A. Lillegraven, Survival in the first hours of the Cenozoic. *Geol. Soc. Am. Bull.* **116**, 760–768 (2004).
104. D. S. Robertson, W. M. Lewis, P. M. Sheehan, O. B. Toon, K-Pg extinction patterns in marine and freshwater environments: The impact winter model. *J. Geophys. Res. Biogeosci.* **118**, 1006–1014 (2013).
105. P. H. Brice, Thermoregulation in monotremes: Riddles in a mosaic. *Aust. J. Zool.* **57**, 255–263 (2009).
106. T. Ruf, F. Geiser, Daily torpor and hibernation in birds and mammals. *Biol. Rev.* **90**, 891–926 (2015).
107. A. S. Blix, Adaptations to polar life in mammals and birds. *J. Exp. Biol.* **219**, 1093–1105 (2016).
108. M. O. Woodburne, T. H. Rich, M. S. Springer, The evolution of tribospheny and the antiquity of mammalian clades. *Mol. Phylogenet. Evol.* **28**, 360–385 (2003).
109. G. W. Rougier, A. G. Martinelli, A. M. Forasiepi, M. J. Novacek, New Jurassic mammals from Patagonia, Argentina: A reappraisal of australosphenidan morphology and interrelationships. *Am. Mus. Novit.* **3566**, 1–54 (2007).
110. P. Goloboff, S. Catalano, TNT version 1.5, including a full implementation of phylogenetic morphometrics. *Cladistics* **32**, 221–238 (2016), 10.1111/cla.12160F.
111. W. P. Maddison, D. R. Maddison, Mesquite: A modular system for evolutionary analysis. <http://www.mesquiteproject.org> (Version 3.70, 2021).
112. G. Savio, R. Meneghello, G. Concheri, Optical properties of spectacle lenses computed by surfaces differential quantities. *Adv. Sci. Lett.* **19**, 595–600 (2013).
113. R. Straehl, T. M. Scheyer, A. M. Forasiepi, R. D. MacPhee, M. R. Sañchez-Villagra, Evolutionary patterns of bone histology and bone compactness in xenarthran mammal long bones. *PLoS One* **8**, e69275 (2013).
114. J. J. Derbridge, E. E. Posthumus, H. S. Chen, J. L. Koprowski, *Solenodon paradoxus* (Soricomorpha: Solenodontidae). *Mamm. Species* **47**, 100–106 (2015).
115. N. P. Myhrvold *et al.*, Diving dinosaurs? Caveats on the use of bone compactness and pFDA for inferring lifestyle. *PLoS One* **19**, e029895 (2024).
116. R. Motani, L. Schmitz, Phylogenetic versus functional signals in the evolution of form-function relationships in terrestrial vision. *Evolution* **65**, 2245–2257 (2011).
117. M. G. Elliot, A. Ø. Mooers, Inferring ancestral states without assuming neutrality or gradualism using a stable model of continuous character evolution. *BMC Evol. Biol.* **14**, 226 (2014).